Polymer Bulletin
https://doi.org/10.1007/s00289-021-03688-9

ORIGINAL PAPER

Isotherms, kinetics and thermodynamics of pb(ii) adsorption by crosslinked chitosan/sepiolite composite

Dilek Senol-Arslan[1]

Received: 30 December 2020 / Revised: 2 March 2021 / Accepted: 26 March 2021

Abstract

A novel composite adsorbent was prepared from chitosan (Ch) and sepiolite (S) for removal of Pb(II) from aqueous solution. The Ch-S composite beads were successfully synthesized by crosslinking epichlorohydrin (ECH) and tripolyphosphate (NaTPP). A number of physicochemical parameters such as, pH, initial Pb(II) concentration, temperature, contact time and desorption have been studied during the adsorption process. Experimental data acquired from batch adsorption tests have been analyzed by three isotherm models (Langmuir, Freundlich and Dubinin–Radushkevich), and three kinetic models including the pseudo-first-order, the pseudo-second-order and intraparticle diffusion equations using nonlinear regression technique. Langmuir isotherm was the best to fit the experimental data ($R^2 = 0.971$). The maximum adsorption capacity was 0.158 mol kg^{-1} from Langmuir isotherm model. Maximum removal efficiency was found approximately 66% for the initial Pb(II) concentration of 1000 mg/L, adsorbent dosage of 100 mg and agitation speed of 150 rpm at pH 4.5. The adsorption free energy was found as E_{DR} (15.8 kJ mol^{-1}), which indicated that Pb(II) adsorption process onto Ch-S composite was chemically performed. The kinetic studies have shown that the best fitted kinetic model is the pseudo-first order ($R^2 = 0.979$). Adsorption enthalpy value was determined as 18.7 kJ mol^{-1}, adsorption entropy was found as 106 J mol^{-1} K^{-1}, and Gibbs free energy was found as 12.9 kJ mol^{-1}. The thermodynamic parameters showed that the adsorption of Pb(II) on Ch-S was endothermic, possible and spontaneous.

Keywords Chitosan · Sepiolite · Composite · Adsorption · Pb (II) · Thermodynamic · Kinetic

✉ Dilek Senol-Arslan
dilek.senol@agu.edu.tr

[1] Nanotechnology Engineering Department, Engineering Faculty, Abdullah Gül University, Kayseri, Turkey

Published online: 13 April 2021

Introduction

The pollution of the environment (water, soil, air and others) with heavy metals is a result of some activities such as industrial, metallurgical and mining. The heavy metal elements like lead (Pb), mercury (Hg), cadmium (Cd), nickel (Ni), thallium (Tl) contaminated soil and water threat to human, animal and plant health [1, 2]. Among these heavy metal ions, lead pollution is the major problem due to lead pipes [3] lead ore mining and smelting [4] leaded gasoline [5, 6]. Additionally, the presence of lead ions in aqueous medium has become a major problem due to their harmful effects on human health, animals and plants [7–9]. Therefore, essential to remove Pb(II) from wastewater before disposal. For this reasons, numerous techniques are used for the removal of lead ions from aqueous solution such as adsorption, solvent extraction, flocculation, chemical precipitation, ion exchange, coagulation and reverse osmosis [10–16]. Among these methods, the adsorption is considered to be the most favorable one. It has significant advantages such as low cost, high selectivity, efficiency, environmental friendliness and ease of application [17]. In order to effectively apply the adsorption method, the material as an adsorbent should be an economical, easily accessible, recyclable and non-toxic material [18, 19]. For this purpose, researchers tend to use non-toxic, cheap, abundant in nature and low-cost adsorbents [20, 21].

Several theories have been proposed to investigate the removal of heavy metal ions from industrial wastewater; natural minerals and polymers such as sea nodule [22], pomegranate peel [23], sphagnum moss peat [24], carbon nanotubes [25, 26], coffee grounds [27], agricultural waste [28], zeolite-kaolin-bentonite [29], clinoptilolite-zeolite [30] Ni-based metal–organic framework [31], yttrium silicate [32], halloysite/graphene quantum dots magnetic nanocomposite [33], biochar [34] and synthetic wastewater [35] are commonly used as adsorbents.

Chitosan (Ch) is a water-soluble aminopolysaccharide obtained by deacetylation of the most abundant kit after cellulose in nature. The chitosan, which has antibacterial and antifungal properties, is nowadays used in various sectors such as textiles, cosmetics, medical uses and agricultural areas [36–38]. Hydroxyl (-OH) and amino ($-NH_2$) groups in the structure of chitosan are active sites for the removal of heavy metals [39–41]. However, chitosan has the disadvantages of being easily soluble in weak acids, poor in thermal stability [42] and difficult to separate [43]. Several chemical and physical methods have been applied to modify the Ch, especially the crosslinking method, which generally used to improve Ch's physicochemical properties such as surface and adsorptive characteristics [44–47]. A series of recent studies has indicated that chitosan-based composites have attracted great attention for their special properties such as adsorption capacity by a crosslinking, chemical stability, surface area and structural properties. The Ch-based composites have been used increasingly in various applications such as an adsorbent biomaterial for the removal of different types of dyes and metal ions [48–51].

Sepiolite $(Si1_2)(Mg_8)O_{30}(OH)_4(OH_2)_4{\cdot}8H_2O$ is a natural clay mineral [52, 53]. The general structure of sepiolite is formed by separating the blocks and tunnels growing in the microfiber direction. Each block consists of two tetrahedral silica

layers connected to the octahedral magnesium layer in the center. However, silica layers are not continuous and reversal of silica layers causes structural tunnels. In addition, sepiolite has a not only high surface area but also high chemical and mechanical stability [54]. The characteristic properties of sepiolite can allow it to be used as adsorbent in adsorbing organic and inorganic ions. However, coagulation and aggregation, which is one of the negativities affecting the hydrodynamic properties of sepiolite, limits its use. These problems can be eliminated by creating a composite of sepiolite.

In this study, a novel Ch-S composite adsorbent was prepared from sepiolite and chitosan with a high adsorption capacity for removal of Pb(II) ions from aqueous solutions. The aims of this study were to: (1) synthesize the composite beads, (2) investigate the adsorption capacities with the help of kinetic, isotherm and thermodynamics parameters and (3) characterize the physical and chemical properties. To our present knowledge, this is the first report about the utilization of Ch-S composite beads, for the adsorption of Pb(II) ions from aqueous solutions.

Materials and methods

Chemicals and devices

In this study, the natural sepiolite (S) was supplied from Akmin Mining (Ankara). Medium molecular weight chitosan (Ch) (Sigma-Aldrich, Germany) was preferred. $(CH_3COO)_2UO_2.2H_2O$, 4-(2-pyridilazo) resorcinol (PAR), Epichlorohydrin (ECH), sodium tripolyphosphate (NaTPP) and the other chemicals were achieved from Merck (Germany). DI water is used in all dilutions and experiments. Spectrophotometric analysis was carried out by a UV–vis spectrophotometer (UV-DR-6000; Shimadzu, China).

The surface of unloaded and Pb(II) loaded Ch-S composite adsorbent were characterized by FT-IR and SEM–EDX analysis. The FT-IR spectra were recorded on a PerkinElmer 400 spectrophotometer. SEM images and EDX compositional data were obtained with a Leo 440 Computer Controlled Digital System.

Preparation of Ch-S composite

Ch-S composite was synthesized according to the following procedure. The typical synthesis procedure applied for chitosan/sepiolite hybrid beads is schematically presented in Fig. 1.

As can be seen in Fig. 1 sepiolite and 2 g chitosan were mixed in acetic acid solution (5% v/v) for 2 h until homogenous mixture was obtained. Then, ECH solution was added to the mixture and ultrasound assisted mixed for 2 h at room temperature. The mixture was lest overnight. Afterward, the mixture was added dropwise to the NaTPP solution to form composite beads. The synthesized composite beads were precipitated and washed three times with double distilled water, and then, the composite was dried in the oven at 40 °C, ground and then stored in closed containers.

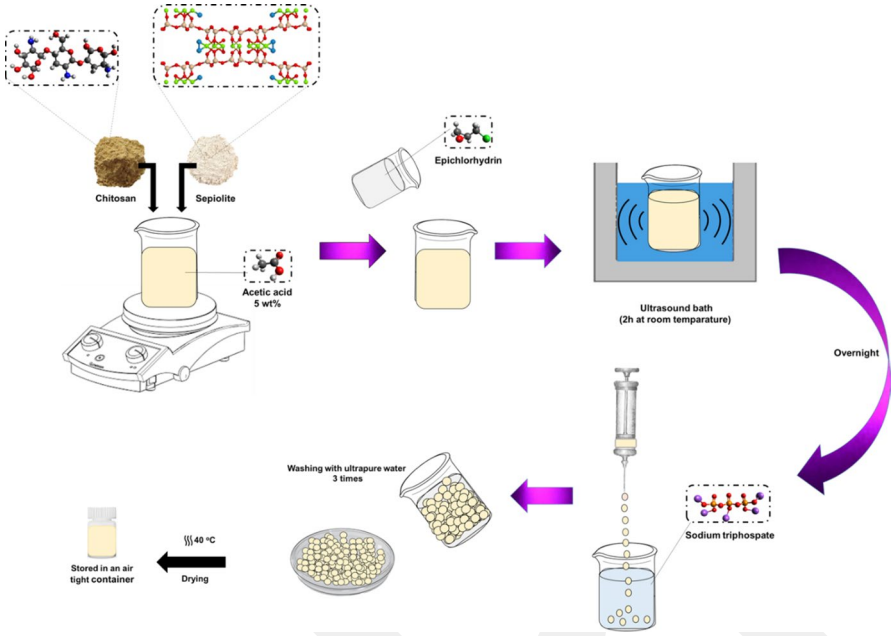

Fig. 1 Shematic illustration for the preparation of chitosan/sepiolite hybrid beads

Methods of analysis

Pb(II) adsorbed on the Ch-S composite was determined with PAR method [55]. With using this method, the concentration of Pb(II) was analyzed by UV–vis spectrophotometer at $\lambda = 520$ nm.

Batch adsorption experiments

Adsorption experiments were carried out at room temperature using the batch method. Stock solution of Pb(II) (5000 mg L^{-1}) was prepared with using distilled water. The adsorbent-solution systems were equilibrated with 1000 mg L^{-1} (3.7×10^{-3} mol L^{-1}) Pb(II) concentration at natural pH 4.5, for 1440 min at 25 °C in 10 mL polypropylene tubes containing 10 mL of Pb(II) solution. The pH value was adjusted by 0.1 mol L^{-1} NaOH and HCl. The batch adsorption conditions are presented in Table 1. Adsorption% and Q (mol kg^{-1}) were calculated with Eqs. 1 and 2 .

$$\text{Adsorption\%} = \left[\frac{C_i - C_f}{C_i}\right] \times 100 \tag{1}$$

Table 1 Experimental conditions for adsorption of Pb(II) onto Ch-S

Experimental conditions					
Aim of experiment	Solution pH	Initial Pb(II) conc. (mg L^{-1})	Adsorbent dosage (g L^{-1})	Contact time (min)	Temperature (°C)
Effect of pH	1.0–7.0	1000	100	1440	25
Effect of concentration	4.5	50–1000	100	1440	25
Effect of time	4.5	1000	300	2–1440	25
Effect of temperature	4.5	1000	100	1440	5, 25, 40
Desorption	4.5	1000	100	1440	25

$$Q = \left[\frac{C_i - C_f}{m}\right] \times V \tag{2}$$

where C_i is the initial concentration (mg L^{-1}), m refers to the adsorbent mass (g), C_f is equilibrium concentration (mg L^{-1}), and V is the solution volume (L).

Desorption experiments

Desorption studies were performed for adsorbent reuse in adsorption processes. In this study, dilute 1 mol L^{-1} HCl, NaOH, HNO_3 and ethanol solutions were used for desorption of the Pb(II) ions from the surface of the Ch-S. In order to determine the desorption property of the Ch-S composite adsorbent, the experiments were repeated three times with the same adsorbent for the adsorbent/desorption cycle. At the end of each experiment, the solutions were centrifuged at 5000 rpm for 10 min to ensure liquid–solid separation and the amount of Pb(II) ions in the equilibrium solution was determined by the UV–vis spectrophotometric method. % Desorption was calculated with Eq. 3.

$$\text{Desorption}\% = \frac{Q_{\text{des}}}{Q_{\text{ads}}} \times 100 \tag{3}$$

In these equation, Q_{des}: desorbed amount of adsorbate (mol kg^{-1}), Q_{ads}: adsorbed amount of adsorbate (mol kg^{-1}).

Results and discussion

FT-IR and SEM analysis

The FT-IR spectra of the Ch, S and Ch-S composites are given in Fig. 2. When the chitosan spectrum was examined, it is observed that the absorption band at

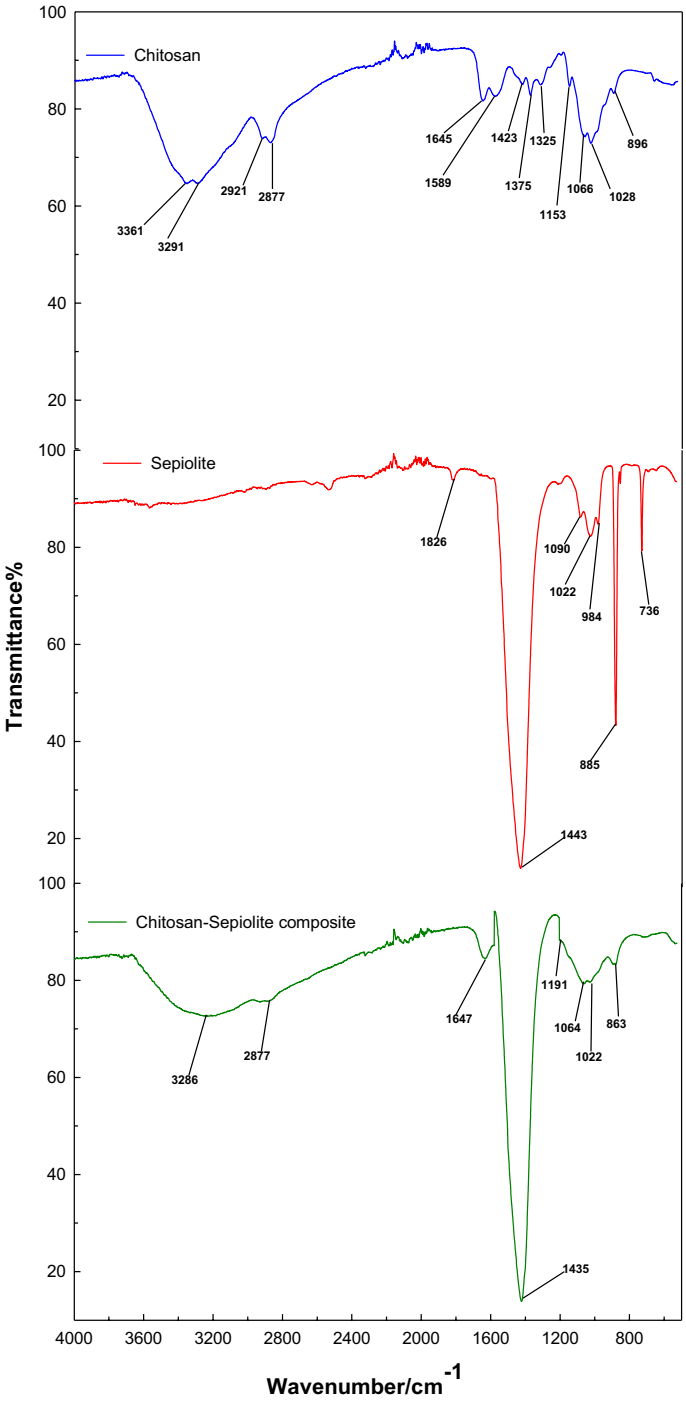

Fig. 2 FT-IR spectra of Ch, S and Ch-S composite

3291–3261 cm^{-1} is assigned to N–H and O–H stretching, the peaks at 2921 and 2877 cm^{-1} is corresponded to C-H symmetric and asymmetric stretching, 1645 cm^{-1} is assigned to C = O stretching of amide I, 1589 cm^{-1} is corresponded to the N–H bending of the primary amine, 1423 and 1375 cm^{-1} is assigned to the CH_2 bending and CH_3 symmetrical deformations, 1325 cm^{-1} is assigned to C-N stretching of amide III, 1550 cm^{-1} is corresponded to N–H bending of amide II, 1153 cm^{-1} is assigned to asymmetric stretching of the C–O–C bridge, 1066–1028 cm^{-1} is assigned to C–O stretching, which are characteristic peaks for chitosan [56–58]. When the sepiolite spectrum was examined, it is observed that the absorption band at 1826 cm^{-1} is assigned to H–O–H stretching vibrations of water molecules weakly hydrogen bonded to the Si–O surface and sepiolite water, while the peak at 1443 cm^{-1} was known as the carbonate peak. The peaks in the 1090–984 cm^{-1} is corresponded to silicates (Si–O–Si and Si–O). The peaks at 885–736 cm^{-1} are assigned to magnesium hydroxides. 984 cm^{-1} is corresponded to the Si–O stretching, 1022 cm^{-1} is assigned to the basal plane of the tetrahedral units indicating the Si–O–Si plane vibrations [59, 60].

When the FT-IR spectrum of Ch-S composite is examined, it is seen that it is different from both spectra. Although the characteristic peaks of both components are observed in the spectrum of the composite, in particular the further expansion of the peak in the range of 700–1600 cm^{-1} is evident that the overlap of the peaks of both components occurred in this wave number. Therefore, FT-IR spectra of Ch-S composite indicated that the Ch-S composite confirm hybrid material of chitosan and sepiolite.

SEM analysis was performed to investigate the surface morphology of Ch-S composite. The SEM photographs of the Ch, S and Ch-S composites are given in Fig. 3a–c.

SEM photographs of Fig. 3a showed that chitosan has a nonporous, smooth membranous phase consisting of dome-shaped orifices, microfibrils and crystallite [61]. Figure 3b shows a typical composition of sepiolite, which has a needle-like fibrous structure. In the literature, natural sepiolite has poor dispersibility because of the hydrogen bonding and van der Waals forces between needle-like crystals in structure of it [62, 63]. SEM photographs of Fig. 3c shows that Ch-S composite shows

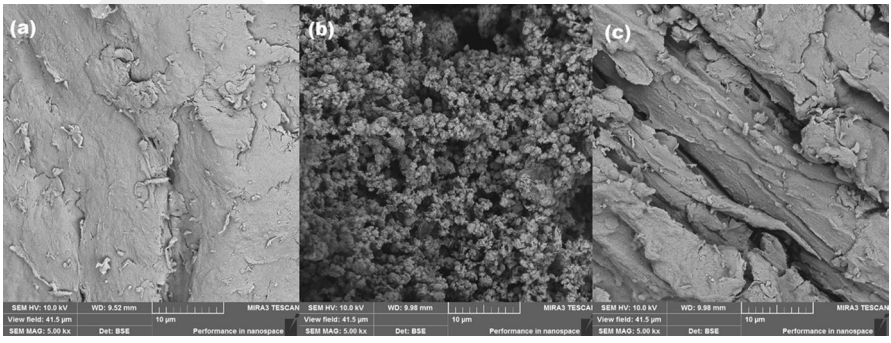

Fig. 3 SEM photographs of chitosan **a**, sepiolite **b** and Ch-S composite **c**

a structure having the hybrid structure of both chitosan and sepiolite. Surface morphology, which is different in the components of the Ch-S composite, was evaluated as evidence that the hybrid composite was synthesized.

Effect of solution pH

The adsorption mechanism is related to the physicochemical interactions of the species in solution. The pH of the aqueous solution is a significant parameter affecting the adsorption process. The pH of the solution is related to the competitiveness of H^+ with Pb(II) to the functional groups on the adsorbent surface. At high acidic pHs, metal cations and hydrogen ions compete for binding to active sites, resulting in less adsorption of metal. At high basic pHs, soluble hydroxide complexes of metal ions are formed. so the adsorption is reduced. As shown in Fig. 4, Pb(II) adsorption capacity increased from 0.062 to 0.232 mol kg^{-1} when the pH 1.0 to 5.0 At high acidic pHs, Pb(II) and H^+ ions competition for binding to active sites, resulting in less adsorption of Pb(II). The maximum amount of adsorbed lead (0.232 mol kg^{-1}) is observed at pH 5.0. At the pHs > 5 values, the adsorption amount decreased with increasing pH. The pH > 5 values have not been studied due to the precipitation behavior of forming hydroxides of lead ions in the solutions [64].

Adsorption isotherms

The adsorption of Pb(II) ions onto Ch-S composite adsorbent was modeled using the Langmuir, Freundlich and Dubinin–Radushkevich (D–R) isotherm models. The Langmuir isotherm theory assumes that adsorption takes place at specific

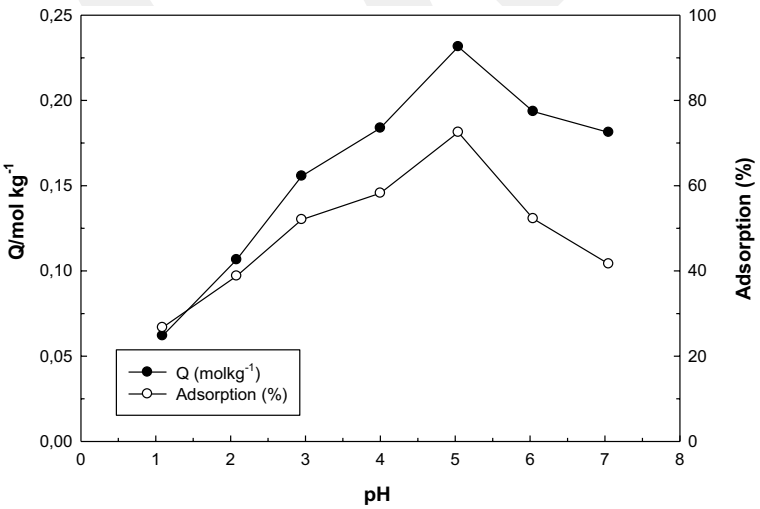

Fig. 4 Effect of pH on the adsorption of Pb(II) onto Ch-S (at 25 °C; adsorbent dose: 100 mg; pH: 1.0–7.0, C_0: 1000 mg L^{-1}; contact time:1440 min)

homogeneous sites within the adsorbent and that adsorption is monolayer [65]. The Freundlich isotherm theory assumes that adsorption occurs on heterogeneous surfaces. The D–R isotherm model examines adsorption energetically [66] The Langmuir, Freundlich and D–R isotherm equations are expressed by following Eqs. 4, 5, and 6 respectively.

$$Q = \frac{X_L K_L C_e}{1 + K_L C_e} \tag{4}$$

$$Q = K_F C_e^n \tag{5}$$

$$Q_e = Q_{\mathrm{DR}} e^{-K_{\mathrm{DR}} \varepsilon^2} \tag{6}$$

where Q is equilibrium uptake (mol kg^{-1}), X_L is the adsorption capacity, K_L is the parameter for Langmuir isotherm, C_e is the equilibrium concentration (mol L^{-1}), K_F is Freundlich constant and n is adsorbent surface heterogeneity. X_{DR} is a measure of adsorption capacity, ε is the Polanyi potential coefficient (mol^2 KJ^2) and K_{DR} is the activity, T is the Kelvin temperature (K), and R is the ideal gas constant (8.314 J mol^{-1} K^{-1}). The Polanyi potential (ε) is expressed by following Eq. 7:

$$\varepsilon = \mathrm{RT} \ln \left(1 + \frac{1}{C_e}\right) \tag{7}$$

The adsorption energy (E) is expressed by the following

$$E_{\mathrm{DR}} = \left(2K_{\mathrm{DR}}\right)^{-0.5} \tag{8}$$

If the adsorption energy is $8 < E < 16$ kJ mol^{-1}, the adsorption is physically controlled and $E < 8$ kJ mol^{-1} indicates that the adsorption proceeds physically (11,12). The harmony to the Langmuir, Freundlich and Dubinin–Radushkevich isotherm models is presented in Fig. 5 and Table 2 show the parameters used in the adsorption isotherms.

The value of correlation coefficient (R^2) of Langmuir model was higher than Freundlich model. Pb(II) adsorption onto Ch-S was more fitted the Langmuir model. Maximum adsorption capacity was calculated to be 0.158 mol kg^{-1} from Langmuir isotherm model. A measurement of adsorption capacity K_F 1.49 and n surface heterogeneity 0.369 from the Freundlich model was found. The Freundlich parameter n indicates the degree of heterogeneity of the surface and the E_{DR} value found in the D-R model indicates that the adsorption process is chemical.

Adsorption kinetics

The kinetic study is very important in batch experiments to find the optimum interaction time of metal ions with adsorbent. The three most commonly kinetics models were used to evaluate the contact time dependence of adsorption process. In order to investigate the adsorption of PB(LL)ions onto Ch-S composite adsorbent were

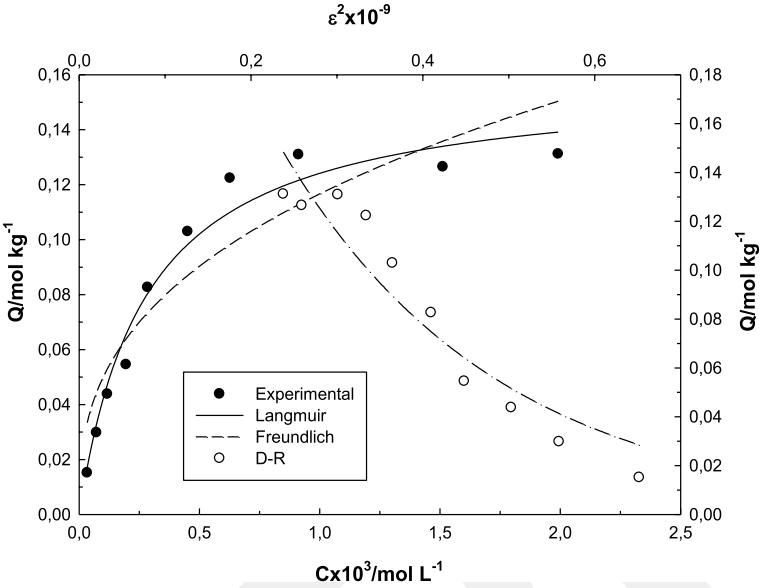

Fig. 5 Experimentally obtained adsorption isotherms of Pb(II) onto Ch-S (at 25 °C; adsorbent dose:100 mg; natural pH:4.5, C_0:50–1000 mg L^{-1}; contact time:1440 min)

Table 2 Langmuir, Freundlich and Dubinin–Radushkevich isotherm models parameters

Langmuir			Freundlich			Dubinin–Radushkevich			
X_L	K_L	R^2	K_F	n	R^2	X_{DR}	$-K_{DR}$ x 10^9	E_{DR}	R^2
0.158	3615	0.971	1.49	0.369	0.867	0.383	3.89	15.8	0.902

X_L(mol kg^{-1}); K_L(L mol^{-1});sub_{DR}(mol kg^{-1}); $-K_{DR}x10^9$ (mol^2KJ^{-2}); E_{DR}(kJ mol^{-1}), Standard deviation 0.045 mol kg^{-1}, standard error 0.0142 mol kg^{-1}

described by pseudo-first-order (PFO), pseudo-second-order (PSO) and intraparticle diffusion (IPD) kinetic models equations (Eq. 9) [67], Eq. 10 [68] and Eq. 11 [69], respectively.

$$Q_t = Q_e\left[1 - e^{-k_1 t}\right] \tag{9}$$

$$Q_t = \frac{t}{\left[\frac{1}{k_2 Q_e^2}\right] + \left[\frac{t}{Q_e}\right]} \tag{10}$$

$$Q_t = k_i t^{0.5} \tag{11}$$

where Q_t (mol kg^{-1}) is the lead absorbed amount at time t (min), Q_e (mol kg^{-1}) is the absorbed amount at equilibrium, k_1, k_2 and k_i are the rate constants for

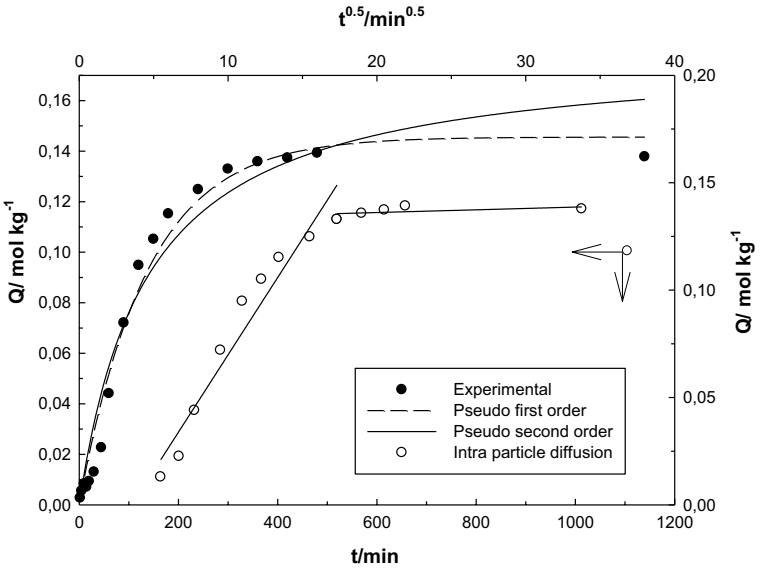

Fig. 6 Compatibility of Pb(II) adsorption kinetics to pseudo-first-order, pseudo-second-order and intra-particle diffusion models (at 25 °C; adsorbent dose: 300 mg; natural pH: 4.5, C_0: 1000 mg L^{-1}; contact time: 2–1440 min)

Table 3 Parameters derived from the compatibility of pseudo-first-order kinetic, pseudo-second-order kinetic and intraparticle diffusion models

Pseudo-first-order kinetic				
Q_t/(mol kg^{-1})	Q_e/(mol kg^{-1})	R^2	$k_1 \times 10^3$/(dk^{-1})	$H \times 10^3$/(mol kg^{-1} min^{-1})
0.146	0.146	0.979	7.34	1.07
Pseudo-second-order kinetic				
Q_t/(mol kg^{-1})	Qe_e/(mol kg^{-1})	R^2	$k_2 \times 10^3$/(mol^{-1}kg min^{-1})	Hx10^3/ (mol kg^{-1} min^{-1})
0.146	0.179	0.956	42.1	1.32
Intraparticle diffusion				
	R^2	$k_i \times 10^3$/ (mol kg^{-1} $min^{-0.5}$)		
	0.885	132		

*Standard deviation 0.057 mol kg^{-1}, standard error 0.0134 mol kg^{-1}

the PFO model (min^{-1}), the PSO model (mol^{-1} kg min^{-1}) and the intra-IPD (mol^{-1} kg $min^{-0.5}$) model, respectively. Adsorption data for kinetics studies were performed in the time range of 2–1440 min. The adsorption kinetics of Pb(II) onto Ch-S composite adsorbent is presented in Fig. 6 and Table 3. The value of correlation coefficient (R^2) of PFO kinetic model was higher than PSO kinetic model. From the harmony of theoretically calculated Q_t and experimental Q_e values, it was

concluded that the PFO model was a suitable model for the adsorption kinetics of Pb(II) ions onto Ch-S composite adsorbent. These finding confirmed that the rate controlling step of adsorption is chemical adsorption.

Adsorption thermodynamics

Thermodynamic parameters are necessary to explain whether the biosorption process is spontaneous or not. Enthalpy and entropy (ΔH^0 and ΔS^0) are obtained from $\ln K_D$ against $1/T$ the graph. The change of Gibbs free energy (ΔG^0) is acquired by Eq. 15. ΔG^0, ΔS^0 and ΔH^0 [70] were calculated using the following equations (Eqs. 12, 13 and 14, respectively);

$$K_D = \frac{Q}{C_e} \tag{12}$$

$$\Delta G = -\mathrm{RT} \ln K_D \tag{13}$$

$$\ln K_D = \frac{\Delta S^0}{R} - \frac{\Delta H^0}{\mathrm{RT}} \tag{14}$$

$$\Delta G^0 = \Delta H^0 - T\Delta S^0 \tag{15}$$

In order to explain the thermodynamic behavior of Pb(II) ions adsorption onto the Ch-S composite, it was studied at temperatures of 5 °C, 25 °C and 40 °C, and Fig. 7 was obtained.

Adsorption enthalpy value was determined as 18.7 kJ mol^{-1} and adsorption entropy was found as 106 J mol^{-1} K^{-1}. The positive of enthalpy and entropy indicate that the adsorption process on Ch-S was endothermic in nature and the randomness was entropy-driven process. With the increase in temperature the value of Gibbs free energy value decreased, this situation indicated that Pb(II) ions adsorption onto the Ch-S was very efficient, spontaneous and possible at higher temperatures. Moreover, the increasing temperature most probably influenced the internal structure of the Ch-S and facilitated the Pb(II) ion distribution in Ch-S composites interspaces structure [71–73].

Desorption

Desorption investigated the reuse ability for Pb(II) ions onto Ch-S composite adsorbent. The Ch-S composite were regenerated using HCl, NaOH, HNO_3 and ethanol. The obtained Pb(II) removal efficiency for three times is plotted in Fig. 8. The maximum recovery percentage for Pb(II) ions onto Ch-S composite adsorbent was achieved with HCl (79%). The minimum recovery percentage for Pb(ll)ions onto Ch-S composite adsorbent was achieved with ethanol (1.5%).

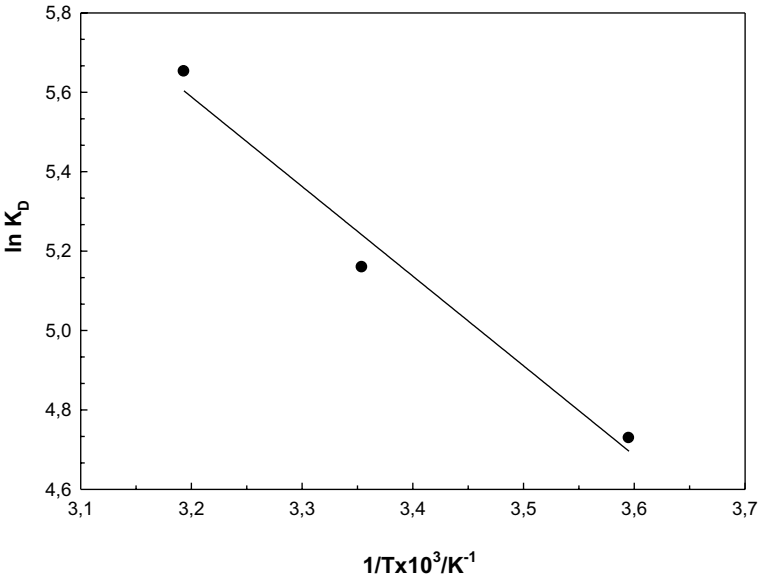

Fig. 7 Effect of temperature on the adsorption of Pb(II) onto Ch-S (at 5 °C, 25 °C, 40 °C; adsorbent dose: 100 mg; natural pH: 4.5, C_0: 1000 mg L^{-1}; contact time: 1440 min)

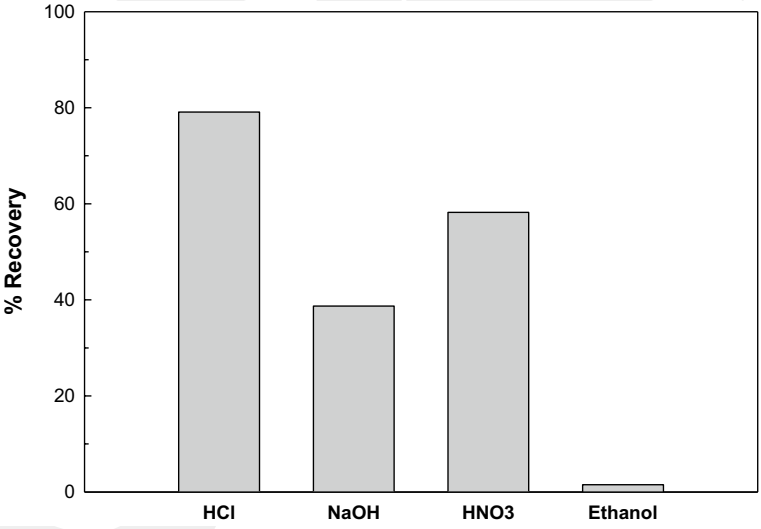

Fig. 8 Recovery rates of various solvents for desorption of Pb(II) (at 25 °C; adsorbent dose:300 mg; natural pH: 4.5, C_0: 1000 mg L^{-1}; contact time: 1440 min)

Comparison of results with literature

The reported studies about the Pb(II) adsorption capacities of various adsorbents are presented in Table 4.

Data in Table 4 reveal that the Ch-S adsorbent can be effectively utilized for the adsorption of Pb(II) ions from aqueous solutions.

Conclusion

In this paper, Ch-S composite adsorbent was successfully synthesized and, then, used for the Pb(II) ions removal from aqueous solution. The obtained results can be summarized as follows:

- The batch studies indicated that optimum working parameters for maximum adsorption were found as pH of the solution: 4.5, adsorbent dosage: 100 mg, contact time: 1440 min and temperature: 25 °C.
- Adsorption isotherm models showed that adsorption of Pb(II) on Ch-S was more appropriate the Langmuir model. The maximum adsorption capacity was 0.158 mol kg^{-1} from Langmuir isotherm model. The adsorption free energy was found as E_{DR} (15.8 kJ mol^{-1}), which indicated that Pb(II) adsorption process onto Ch-S composite was chemically performed.
- According to adsorption kinetics, the value of correlation coefficient (R^2) and the harmony of theoretically calculated Q_t and experimental Q_e values was concluded that the PFO model was a suitable model for the adsorption kinetics of Pb(II) ions onto Ch-S composite adsorbent. These finding confirmed that the rate controlling step of adsorption is chemical adsorption.

Table 4 Comparison of adsorption capacities of different adsorbents for the removal of Pb(II) ions

Adsorbent	Max. adsorption capacity, /mol kg^{-1}	References
Chitosan/hydroxyapatite	0.060	[74]
Graphene oxide	0.536	[75]
Carbon nanotubes	0.492	[76]
Otostegia persica waste biomass	0.0835	[77]
Alginate-melamine hybrid	1.389	[78]
Silica-modified calcium alginate-xanthan gum hybrid bead composite	0.091	[79]
Chitosan/graphene oxide	0.543	[80]
Chitosan/vermiculite	0.154	[55]
Chitosan/sepiolite	0.158	This study

- Adsorption enthalpy value was determined as 18.7 kJ mol^{-1}, adsorption entropy was found as 106 J mol^{-1} K^{-1}, and Gibbs free energy was found as 12.9 kJ mol^{-1}. Thermodynamic parameters of adsorption showed that Pb(II) ions onto Ch-S composite was endothermic, spontaneous and possible.
- The desorption studies have found that Ch-S composite adsorbent has a good adsorption/desorption performance for Pb(II).
- The adsorption process of the Ch-S composite adsorbent shows promise as an improved, simple and inexpensive method for treating water and wastewater.

References

1. Masindi V, Muedi KL (2018) Environmental contamination by heavy metals. Heavy Metals 10:115–132
2. Shawai SAA et al. (2017) A Review on heavy metals contamination in water and soil: effects, sources and phytoremediation techniques. Int J Min Process Extr Metall 2(2):21–27
3. Shiomi, N, An assessment of the Causes of Lead pollution and the efficiency of bioremediation by plants and microorganisms. Advances in Bioremediation of Wastewater and Polluted Soil.: InTech, 2015: p. 247-274.
4. Singh N, Li JH (2014) Environmental impacts of lead ore mining and smelting. In: Advanced Materials Research. Trans Tech Publ 878:338–347
5. Craxford S (1983) Pollution from lead in petrol. Oil Petrochem Pollut 1(4):285–290
6. Bu N et al. (2020) Synthesis of NaY zeolite from coal gangue and its characterization for lead removal from aqueous solution. Adv Powder Technol 31(7):2699–2710
7. Demayo A et al. (1982) Toxic effects of lead and lead compounds on human health, aquatic life, wildlife plants, and livestock. Crit Rev Environ Sci Technol 12(4):257–305
8. Kumar A et al. (2020) Lead Toxicity: Health Hazards, Influence on Food Chain, and Sustainable Remediation Approaches. Int J Environ Res Public Health 17(7):2179
9. Gholinejad, B, et al., Effects of lead ions on germination, initial growth, and physiological characteristics of Lolium perenne L. species and its bioaccumulation potential. Environmental Science and Pollution Research, 2020: p. 1–9.
10. Dong L et al. (2010) Removal of lead from aqueous solution by hydroxyapatite/magnetite composite adsorbent. Chem Eng J 165(3):827–834
11. Idris SA et al. (2011) Large pore diameter MCM-41 and its application for lead removal from aqueous media. J Hazard Mater 185(2–3):898–904
12. Perret S et al. (2000) Polarographic study of the removal of cadmium (II) and lead (II) from dilute aqueous solution by a synthetic flocculant comparison with copper (II) and nickel (II). Water Res 34(14):3614–3620
13. Esalah JO, Weber ME, Vera JH (2000) Removal of lead, cadmium and zinc from aqueous solutions by precipitation with sodium Di-(n-octyl) phosphinate. Canadian J Chem Eng 78(5):948–954
14. Ahmed S, Chughtai S, Keane MA (1998) The removal of cadmium and lead from aqueous solution by ion exchange with NaY zeolite. Sep Purif Technol 13(1):57–64
15. Rashida WT, Alkadira IA, Jalhoom MG (2020) Effect of Operating Conditions on the Removal of Heavy and Radioactive Elements by Reverse Osmosis Membrane. Al-Qadisiyah J Eng Sci 13(3):240–245
16. Meng X et al. (2020) Removal of chemical oxygen demand and ammonia nitrogen from lead smelting wastewater with high salts content using electrochemical oxidation combined with coagulation–flocculation treatment. Sep Purif Technol 235:116233
17. Chakraborty R et al. (2020) Adsorption of heavy metal ions by various low-cost adsorbents: a review. Int J Environ Anal Chem. https://doi.org/10.1080/03067319.2020.1722811
18. Singh S, Wasewar KL, Kansal SK (2020) Low-cost adsorbents for removal of inorganic impurities from wastewater. Inorganic Pollutants in Water. Elsevier, pp 173–203

19. Xiao Z et al. (2020) Simultaneous removal of NO and SO2 with a new recycling micro-nano bubble oxidation-absorption process based on HA-Na. Sep Purif Technol. https://doi.org/10.1016/j.seppur.2020.116788
20. Ahmad N et al. (2020) Chitosan Based Nanocomposites as Efficient Adsorbents for Water Treatment. Modern Age Waste Water Problems. Springer, pp 69–83
21. Zhang S et al. (2020) Fabrication of L-cysteine stabilized α-FeOOH nanocomposite on porous hydrophilic biochar as an effective adsorbent for Pb2+ removal. Sci Total Environt. https://doi.org/10.1016/j.scitotenv.2020.137415
22. Bhattacharjee S et al. (2003) Removal of lead from contaminated water bodies using sea nodule as an adsorbent. Water Res 37(16):3954–3966
23. El-Ashtoukhy E-S, Amin NK, Abdelwahab O (2008) Removal of lead (II) and copper (II) from aqueous solution using pomegranate peel as a new adsorbent. Desalination 223(1–3):162–173
24. Ho Y, Wase D, Forster C (1996) Removal of lead ions from aqueous solution using sphagnum moss peat as adsorbent. WATER SA-PRETORIA- 22:219–224
25. Gupta VK, Agarwal S, Saleh TA (2011) Synthesis and characterization of alumina-coated carbon nanotubes and their application for lead removal. J Hazard Mater 185(1):17–23
26. Li Y-H et al. (2006) Different morphologies of carbon nanotubes effect on the lead removal from aqueous solution. Diam Relat Mater 15(1):90–94
27. Seniūnaitė, J Vaiškūnaitė,R and Bolutienė R (2014) Coffee grounds as an adsorbent for copper and lead removal form aqueous solutions. In :The 9th International Conference " ENVIRONMENTAL ENGINEERING", VGTU Press. 2014.
28. Ibrahim MM et al. (2010) A novel agricultural waste adsorbent for the removal of lead (II) ions from aqueous solutions. J Hazard Mater 182(1–3):377–385
29. Salem A, Sene RA (2011) Removal of lead from solution by combination of natural zeolite–kaolin–bentonite as a new low-cost adsorbent. Chem Eng J 174(2–3):619–628
30. Aghel B et al. (2020) Use of modified Iranian clinoptilolite zeolite for cadmium and lead removal from oil refinery wastewater. Int J Environ Sci Technol 17(3):1239–1250
31. Farahani SD, Zolgharnein J (2020) Multivariate optimization of high removal of lead (II) using an efficient synthesized Ni-based metal–organic framework adsorbent. Chinese J Chem Eng 29:146–153
32. Medeiros VL et al. (2020) Synthesis and physicochemical characterization of a novel adsorbent based on yttrium silicate: a potential material for removal of lead and cadmium from aqueous media. J Environ Chem Eng. https://doi.org/10.1016/j.jece.2020.103922
33. Pirhaji JZ et al. (2020) Synthesis and characterization of halloysite/graphene quantum dots magnetic nanocomposite as a new adsorbent for Pb (II) removal from water. J Mol Liq 300:112345
34. Gao J et al. (2020) A promising and cost-effective biochar adsorbent derived from jujube pit for the removal of Pb (II) from aqueous solution. Sci Rep 10(1):1–13
35. Onundi Y et al. (2011) Heavy metals removal from synthetic wastewater by a novel nano-size composite adsorbent. Int J Environ Sci Technol 8(4):799–806
36. Lim S-H, Hudson SM (2003) Review of chitosan and its derivatives as antimicrobial agents and their uses as textile chemicals. Journal of macromolecular science, part C: Polymer reviews 43(2):223–269
37. Dutta, PK, Dutta J, and Tripathi V (2004) Chitin and chitosan: Chemistry, properties and applications. 2004.
38. Hernández-Téllez CN, Plascencia-Jatomea M, Cortez-Rocha MO (2016) Chitosan-based bionanocomposites: development and perspectives in food and agricultural applications. Chitosan in the preservation of agricultural commodities. Elsevier, pp 315–338
39. Colmenares JC, Kuna E (2017) Photoactive hybrid catalysts based on natural and synthetic polymers: a comparative overview. Molecules 22(5):790
40. Peng H-L et al. (2019) Chitosan-derived mesoporous carbon with ultrahigh pore volume for amine impregnation and highly efficient CO2 capture. Chem Eng J 359:1159–1165
41. Prasad B, Mandal B (2018) Preparation and characterization of CO2-selective facilitated transport membrane composed of chitosan and poly (allylamine) blend for CO2/N2 separation. J Ind Eng Chem 66:419–429
42. Ilium L (1998) Chitosan and its use as a pharmaceutical excipient. Pharm Res 15(9):1326–1331
43. Singla A, Chawla M (2001) Chitosan: Some pharmaceutical and biological aspects-an update. J Pharm Pharmacol 53(8):1047–1067

44. Mohammed IA et al. (2020) Physicochemical modification of chitosan with fly ash and tripolyphosphate for removal of reactive red 120 dye: Statistical optimization and mechanism study. Int J Biol Macromol 161:503–513
45. Jawad AH, Abdulhameed AS, Mastuli MS (2020) Mesoporous crosslinked chitosan-activated charcoal composite for the removal of thionine cationic dye: comprehensive adsorption and mechanism study. J Polym Environ 28(3):1095–1105
46. Jawad AH, Mohammed IA, Abdulhameed AS (2020) Tuning of Fly Ash Loading into Chitosan-Ethylene Glycol Diglycidyl Ether Composite for Enhanced Removal of Reactive Red 120 Dye: Optimization Using the Box-Behnken Design. J Polym Environ 28(10):2720–2733
47. Jawad AH, Mubarak NSA, Abdulhameed AS (2020) Tunable Schiff's base-cross-linked chitosan composite for the removal of reactive red 120 dye: adsorption and mechanism study. Int J Biol Macromol 142:732–741
48. Jawad AH et al. (2020) Adsorptive performance of carbon modified chitosan biopolymer for cationic dye removal: kinetic, isotherm, thermodynamic, and mechanism study. Int J Environ Anal Chem. https://doi.org/10.1080/03067319.2020.1807966
49. Jawad AH, Mubarak NSA, Abdulhameed AS (2020) Hybrid crosslinked chitosan-epichlorohydrin/TiO 2 nanocomposite for reactive red 120 dye adsorption: kinetic, isotherm, thermodynamic, and mechanism study. J Polym Environ 28(2):624–637
50. Abd Malek NN et al. (2020) New magnetic Schiff's base-chitosan-glyoxal/fly ash/Fe3O4 biocomposite for the removal of anionic azo dye: An optimized process. Int J Biol Macromol 146:530–539
51. Jawad AH et al. (2020) Statistical optimization and modeling for color removal and COD reduction of reactive blue 19 dye by mesoporous chitosan-epichlorohydrin/kaolin clay composite. Int J Biol Macromol 164:4218–4230
52. Tunç S, Duman O, Çetinkaya A (2011) Electrokinetic and rheological properties of sepiolite suspensions in the presence of hexadecyltrimethylammonium bromide. Colloids Surf A 377(1–3):123–129
53. Duman O, Tunc S, Polat TG (2015) Adsorptive removal of triarylmethane dye (Basic Red 9) from aqueous solution by sepiolite as effective and low-cost adsorbent. Microporous Mesoporous Mater 210:176–184
54. Alvarez A (1984) Sepiolite: properties and uses. Developments in sedimentology. Elsevier, pp 253–287
55. Şenol ZM (2020) Kitosan-Vermikülit Kompoziti Kullanılarak Sulu Çözeltiden Etkin Kurşun Giderimi: Denge, Kinetik ve Termodinamik Çalışmalar. Akademik Platform Mühendislik ve Fen Bilimleri Dergisi 8(1):15–21
56. Vino AB et al. (2012) Extraction, characterization and in vitro antioxidative potential of chitosan and sulfated chitosan from Cuttlebone of Sepia aculeata Orbigny, 1848. Asian Pac J Trop Biomed 2(1):S334–S341
57. Fernandes Queiroz M et al. (2015) Does the use of chitosan contribute to oxalate kidney stone formation? Mar Drugs 13(1):141–158
58. Song H et al. (2013) Folic acid-chitosan conjugated nanoparticles for improving tumor-targeted drug delivery. BioMed Res Int. https://doi.org/10.1155/2013/723158
59. Ongen A et al. (2012) Adsorption of Astrazon Blue FGRL onto sepiolite from aqueous solutions. Desalin Water Treat 40(1–3):129–136
60. Jiang X et al. (2017) Development of organic–inorganic hybrid beads from sepiolite and cellulose for effective adsorption of malachite green. RSC Adv 7(62):38965–38972
61. Kumar S, Koh J (2012) Physiochemical, optical and biological activity of chitosan-chromone derivative for biomedical applications. Int J Mol Sci 13(5):6102–6116
62. Li Y et al. (2018) Effective removal of emulsified oil from oily wastewater using surfactant-modified sepiolite. Appl Clay Sci 157:227–236
63. García-Romero E, Suárez M (2014) Sepiolite-palygorskite polysomatic series: Oriented aggregation as a crystal growth mechanism in natural environments. Am Miner 99(8–9):1653–1661
64. Ilaiyaraja P et al. (2013) Adsorption of uranium from aqueous solution by PAMAM dendron functionalized styrene divinylbenzene. J Hazard Mater 250:155–166
65. Langmuir I (1916) The constitution and fundamental properties of solids and liquids Part I Solids. J Am chem soc 38(11):2221–2295
66. Celebi O et al. (2007) A radiotracer study of the adsorption behavior of aqueous Ba2+ ions on nanoparticles of zero-valent iron. J Hazard Mater 148(3):761–767
67. Cui X et al. (2016) Potential mechanisms of cadmium removal from aqueous solution by Canna indica derived biochar. Sci Total Environ 562:517–525

68. Ho Y, McKay G (1999) Comparative sorption kinetic studies of dye and aromatic compounds onto fly ash. Journal of Environmental Science & Health Part A 34(5):1179–1204
69. Qiu H et al. (2009) Critical review in adsorption kinetic models. Journal of Zhejiang University-Science A 10(5):716–724
70. Milonjić SK (2007) A consideration of the correct calculation of thermodynamic parameters of adsorption. J Serb Chem Soc 72(12):1363–1367
71. Jawad AH, Abdulhameed AS (2020) Facile synthesis of crosslinked chitosan-tripolyphosphate/kaolin clay composite for decolourization and COD reduction of remazol brilliant blue R dye: Optimization by using response surface methodology. Colloids Surf, A 605:125329
72. Jawad AH et al. (2020) Zwitterion composite chitosan-epichlorohydrin/zeolite for adsorption of methylene blue and reactive red 120 dyes. Int J Biol Macromol 163:756–765
73. Sheshmani S et al. (2015) Preparation of graphene oxide/chitosan/FeOOH nanocomposite for the removal of Pb (II) from aqueous solution. Int J Biol Macromol 80:475–480
74. Gupta N, Kushwaha A, Chattopadhyaya M (2012) Journal of the Taiwan Institute of Chemical Engineers composite from aqueous solution. J Taiwan Inst Chem Eng 43:125–131
75. Yari M et al. (2016) Removal of Pb (II) ion from aqueous solution by graphene oxide and functionalized graphene oxide-thiol: effect of cysteamine concentration on the bonding constant. Desalin Water Treat 57(24):11195–11210
76. Kabbashi NA et al. (2009) Kinetic adsorption of application of carbon nanotubes for Pb (II) removal from aqueous solution. J Environ Sci 21(4):539–544
77. Alavi S, Zilouei H, Asadinezhad A (2015) Otostegia persica biomass as a new biosorbent for the removal of lead from aqueous solutions. Int J Environ Sci Technol 12(2):489–498
78. Li K et al. (2018) Efficient removal of lead ions from water by a low-cost alginate-melamine hybrid sorbent. Appl Sci 8(9):1518
79. Zhang S et al. (2013) Silica modified calcium alginate–xanthan gum hybrid bead composites for the removal and recovery of Pb (II) from aqueous solution. Chem Eng J 234:33–42
80. Samuel MS et al. (2018) Adsorption of Pb (II) from aqueous solution using a magnetic chitosan/graphene oxide composite and its toxicity studies. Int J Biol Macromol 115:1142–1150